(4)

GL-TR-89-0145 ARC-TR-89-012

Retrieval of Atomic Oxygen and Temperature in the Thermosphere. 2: Feasibility of an Experiment Based on Limb Emission in the OI Lines

A. S. Zachor
B. K. Yap

Atmospheric Radiation Consultants, Inc.
59 High Street
Acton, Massachusetts 01720

30 May 1989

Final Report
February 1987 through April 1989

APPROVED FOR PUBLIC RELEASE; DISTRIBUTION UNLIMITED

GEOPHYSICS LABORATORY
AIR FORCE SYSTEMS COMMAND
UNITED STATES AIR FORCE
HANSCOM AIR FORCE BASE, MASSACHUSETTS 01731-5000

UNCLASSIFIED

SECURITY CLASSIFICATION OF THIS PAGE

REPORT DOCUMENTATION PAGE

1a REPORT SECURITY CLASSIFICATION UNCLASSIFIED	1b RESTRICTIVE MARKINGS N/A
2a SECURITY CLASSIFICATION AUTHORITY 2b DECLASSIFICATION/DOWNGRADING SCHEDULE	3 DISTRIBUTION/AVAILABILITY OF REPORT Approved for public release; Distribution unlimited
4 PERFORMING ORGANIZATION REPORT NUMBER(S) ARC-TR-89-012	5 MONITORING ORGANIZATION REPORT NUMBER(S) GL-TR-89-0145
6a NAME OF PERFORMING ORGANIZATION Atmospheric Radiation Consultants, Inc.	6b OFFICE SYMBOL (If applicable) 7a NAME OF MONITORING ORGANIZATION Geophysics Laboratory
6c ADDRESS (City, State and ZIP Code) 59 High Street Acton, Massachusetts 01720	7b ADDRESS (City, State and ZIP Code) Hanscom AFB, MA 01731-5000
8a NAME OF FUNDING/SPONSORING ORGANIZATION	8b OFFICE SYMBOL (If applicable) 9 PROCUREMENT INSTRUMENT IDENTIFICATION NUMBER F19628-87-C-0053
8c ADDRESS (City, State and ZIP Code)	10 SOURCE OF FUNDING NOS

PROGRAM ELEMENT NO	PROJECT NO	TASK NO	WORK UNIT NO
61101F	ILIR	7B	AA

11 TITLE (Include Security Classification)
Retrieval of Atomic Oxygen and (Cont.)

12 PERSONAL AUTHOR(S)
A. S. Zachor* and B. K. Yap**

13a TYPE OF REPORT	13b TIME COVERED	14 DATE OF REPORT (Yr, Mo, Day)	15 PAGE COUNT
Final Scientific	FROM Feb 87 TO Apr 89	1989 May 30	40

16 SUPPLEMENTARY NOTATION
*Atmospheric Radiation Consultants, Inc., 59 High St., Acton, MA 01720
**Yap Analytics, Inc., 594 Marrett Rd., Lexington, MA 02173

17 COSATI CODES		
FIELD	GROUP	SUB GR

18 SUBJECT TERMS (Continue on reverse if necessary and identify by block number)
Thermosphere; Limb retrieval; Atomic oxygen density; Remote sensing; Translational temperature; Fabry-Perot

19 ABSTRACT (Continue on reverse if necessary and identify by block number)

A viable technique for remote sensing of the atomic oxygen density and translational temperature profiles above 80 km altitude, where oxygen atoms are involved in important chemical, collisional and radiative cooling processes, would have enormous value. The two profiles can, in principle, be recovered simultaneously from limb scan data obtained near wavelength 147 μm and/or 63 μm, corresponding to the intermultiplet transitions in the ground electronic state of atomic oxygen. Part 1 of this report considered an approach in which the limb radiance data represents just one of the lines observed at high spectral resolution; recovery of the temperature relies mainly on Doppler broadening. Here, in Part 2, we evaluate feasibility of the experiment concept when the data is a pair of limb radiance profiles corresponding to the two unresolved OI lines; temperature retrieval relies mostly on the difference in upper state populations. (Cont.)

20 DISTRIBUTION/AVAILABILITY OF ABSTRACT	21 ABSTRACT SECURITY CLASSIFICATION
UNCLASSIFIED/UNLIMITED ☒ SAME AS RPT ☐ DTIC USERS ☐	Unclassified

22a NAME OF RESPONSIBLE INDIVIDUAL	22b TELEPHONE NUMBER (Include Area Code)	22c OFFICE SYMBOL
R. D. Sharma	(617) 377-4198	GL/OPB

DD FORM 1473, 83 APR EDITION OF 1 JAN 73 IS OBSOLETE

UNCLASSIFIED

SECURITY CLASSIFICATION OF THIS PAGE

Block No. 11 (Continued)

...Temperature in the Thermosphere. 2: Feasibility of an Experiment Based on Limb Emission in the OI Lines

Block No. 19 (Continued)

O-atom density and translational temperature profiles were retrieved from noise-contaminated synthetic data by an inversion procedure that uses both the onion peeling and global-fit methods. The latter allows solutions to be obtained despite the occurrence of a singular Jacobian, typically at 200 km tangent height. It is concluded that stable profiles for the altitude range 90-300 km can be recovered when the noise-equivalent radiances in the two channels are no greater than roughly 10^{-13} W $cm^{-2}sr^{-1}$. We estimate that this level of sensitivity could be achieved in a small spaceborne cryogenic sensor based on non-scanning Fabry-Perot etalons. The spectrally resolved approach described in Part 1 required a considerably larger, more advanced sensor.

PREFACE

This is the second of two reports submitted in fulfillment of the Contract Data Requirements (Line Item 0002) of Contract No. F19628-87-C-0053. The study was funded by the AFGL FY87 In-House Laboratory Research (ILIR) Program and was sponsored by the Air Force Systems Command through the above-referenced Contract.

Scientists and engineers who contributed to the reported research are

A. S. Zachor, Atmospheric Radiation Consultants, Inc.
R. D. Sharma, Geophysics Laboratory/OPB
B. K. Yap, Yap Analytics, Inc.
J. P. Riehl, University of Missouri-St. Louis

We gratefully acknowledge the interest and support of Randall Murphy at GL and of the GL Commander, Col. J. R. Johnson. Valuable insights and motivation were provided by A. T. Stair, Jr. when he was Chief Scientist at GL. Howard Smith, when he was at the Naval Research Laboratory, helped us in analyzing Fabry-Perot system capabilities.

The following papers and reports were written and/or presented under sponsorship of Contract No. F19628-87-C-0053:

R. D. Sharma and A. S. Zachor, "Signal Requirements for Remote IR Limb Sounding of Atomic Oxygen and Temperature in the Thermosphere," presented at the OSA Topical Meeting on Laser and Optical Remote Sensing, 28 Sept. to 1 Oct. 1987, N. Falmouth, MA.

A. S. Zachor and R. D. Sharma, "Simultaneous Retrieval of Atomic Oxygen and Temperature in the Thermosphere by an IR Limb Scanning Technique," presented at the International Workshop on Remote Sensing Retrieval Methods, 15-18 December 1987, Williamsburg, VA. (Conference proceedings in press).

B. K. Yap, "FIR Fabry-Perot Interferometer Design Tradeoffs," Final Report on Subcontract No. 87-010, Yap Analytics, Inc., 594 Marrett Road, Lexington, MA 02173, 24 March 1989.

J. P. Riehl, "Fabry-Perot Limb Sounding of Atomic Oxygen Density and Temperature," Final Report on Subcontract No. 87-020, Dept. of Chemistry, University of Missouri-St. Louis, St. Louis, MO 63121, 30 January 1989.

A. S. Zachor, "Retrieval of Atomic Oxygen and Temperature in the Thermosphere. 1: Feasibility of an Experiment Based

on the Spectrally Resolved 147 μm Limb Emission," Scientific Report No. 1 on Contract No. F19628-87-C-0053, Report No. GL-TR-89-0144, Geophysics Laboratory, Hanscom AFB, MA 01731, April 10, 1989.

A. S. Zachor and R. D. Sharma, "Retrieval of Atomic Oxygen and Temperature in the Thermosphere. 1: Feasibility of an Experiment Based on the Spectrally Resolved 147 μm Limb Emission." Accepted for publication in Planetary and Space Science. (This is an expanded version of Scientific Report No. 1).

1. INTRODUCTION

Atomic oxygen and translational temperature are involved in important chemical and collisional processes in the thermosphere, but existing methods for measuring thermospheric profiles of the O-atom density and translational temperature have serious deficiencies, as pointed out by Zachor and Sharma (1989). Sharma, et al. (1987) proposed to measure the two profiles by a new remote sensing method based on limb radiance data provided by a spaceborne Fabry-Perot system with channels centered at 147 μm and 63 μm wavelength, corresponding to the intermultiplet ground electronic state OI transitions ($^3P_0 \rightarrow {}^3P_1$ and $^3P_1 \rightarrow {}^3P_2$). This report is the second of two that evaluate the feasibility of the proposed experiment concept. The earlier one, an interim report, will be referred to as Part 1, and the present final report as Part 2. The reports evaluate two fundamentally different approaches.

Part 1 analyzed a single-channel version of the proposed technique, in which the limb radiance data corresponds to just one of the OI lines spectrally resolved. It was tested for both the 147 μm and the 63 μm line, using synthetic data corresponding to various levels of signal-to-noise and spectral resolution. The 147 μm line, because it is not as strongly absorbing as the 63 μm line, proved to be the better choice. Application of an onion-peeling technique to the 147 μm synthetic spectral data yielded stable temperature and O-atom density solutions from 300 km down to an altitude between 130 and 90 km, depending on the noise level and spectral resolution.

However, it was determined that a spaceborne Fabry-Perot sensor having the sensitivity and spectral resolution needed for retrievals down to 90 km altitude would require rather large, cooled foreoptics and an advanced etalon design. In particular, the wire mesh etalon would have to be much larger in size than we believe is practicable unless the Fabry-Perot system is confocal, i.e., is based on spherical mesh etalon reflectors. While a confocal etalon providing the required high resolving power ($\sim 5 \times 10^5$) is theoretically possible, this combination of design and performance remains to be demonstrated.

Here, in Part 2, we evaluate an alternative approach in which the data consists of a pair of limb radiance profiles corresponding to the two unresolved OI lines. This approach, and the one evaluated in Part 1, will be referred to hereinafter as the nonresolved and resolved approaches, respectively. In the nonresolved case, recovery of the translational temperature is based physically on the relative OI line intensities, that is, on the relative upper-state populations of the two transitions for the O-atoms in a given volume element. In the resolved case, retrieval of temperature relies on the spectral shape of the volume emission, that is, on Doppler broadening of the 147 μm line.

In evaluating the nonresolved approach, we inverted synthetic limb radiance data that included noise. The retrievals are performed by an algorithm which uses the onion-peeling method (see, e.g., Goldman and Saunders, 1979) over

most of the 300-to-90 km altitude range, and uses the global-fit method (see, e.g., Carlotti, 1988) near 200 km altitude where a singularity causes divergence in the onion-peeling method. An interesting finding of the study is that changes in the OI limb radiances, typically at the tangent height 200 km, due to a perturbation in O-atom density near this altitude, are indistinguishable from changes due to a temperature perturbation; i.e., the four-element Jacobian matrix of radiance partial derivatives is singular. This singularity, which does not occur at other tangent heights, is more easily avoided in the global-fit technique than in the onion-peeling method. Based on the retrieved O-atom density and temperature profiles corresponding to various levels of noise in the synthetic data, we estimate basic system requirements for a spaceborne Fabry-Perot sensor. It is concluded that the non-resolved approach is experimentally feasible using currently available technology.

2. RADIATIVE TRANSFER EQUATIONS

The spectral radiance $N_\nu(z)$ along a path through an emitting and absorbing medium with boundary condition $N_\nu(0) = 0$ is given by

$$N_\nu(z) = \int_0^z \exp\left[-\int_y^z n(x)\ k_\nu(x)\ dx\right] \xi_\nu(y)\ dy/4\pi \qquad (1)$$

where $n(z)$ is the density of the emitting/absorbing species, $k_\nu(z)$ is the absorption coefficient, and $\xi_\nu(z)$ is the spectrally resolved volume emission rate, defined as the number of photons emitted per unit time per unit wavenumber interval per unit volume. The exponential factor in the integrand is the spectral transmittance of path segment yz; this transmittance times $\xi_\nu(y)\ dy/4\pi$ is the contribution of path element dy at point y to the spectral radiance at point z. By applying equation (1) to a path through the limb and evaluating N_ν at a point $z = Z$ above the atmosphere (see Fig. 1), one obtains the limb spectral radiance. In general, k_ν and ξ_ν depend on the path temperature distribution $T(z)$ and pressure distribution $p(z)$. We assume a spherically stratified atmosphere characterized by the vertical profiles $n(H)$ (the O-atom number density, hereinafter denoted [O]), $T(H)$ and $p(H)$. A limb path may then be specified by its tangent height H_T (Fig. 1). A spaceborne sensor, by scanning

the limb, can measure the limb spectral radiance profile $N_\nu(H_T)$ or its nonresolved counterpart $N(H_T)$.

In the present work $N_\nu(H_T)$ refers to the spectral radiance arising from a single OI transition at wavenumber ν_0 (wavelength λ_0 = 147 μm or 63 μm). Associated with the transition is an Einstein coefficient A, upper state statistical weight g_u and upper state energy E_u. Values of A, g_u and E_u for the two OI lines are given in Table 1. The corresponding volume emission rate ξ_ν, assuming LTE, is given by

$$\xi_\nu = A \cdot [O] f(\nu - \nu_0, T, p) g_u \exp(-c_2 E_u / T) / Q(T) \qquad (2)$$

where $f(\nu, T, p)$ is the normalized Voigt shape of the line due to Doppler and collisional broadening, c_2 = 1.4388 K/cm^{-1} is the second radiation constant, and $Q(T)$ is the partition sum,

$$Q(T) = \exp(-c_2 \times 226.5/T) + 3 \exp(-c_2 \times 158.5/T) + 5 \qquad (3)$$

The absorption coefficient is given by

$$k_\nu = f(\nu - \nu_0, T, p)\ S(\nu_0, T) \qquad (4)$$

where S is the line intensity,

$$S(\nu_0, T) = [A/(8\pi c \nu_0^2)][(1-\gamma)/\gamma] g_u \exp(-c_2 E_u / T) / Q(T) \qquad (5)$$

with

$$\gamma = \exp(-c_2\nu_0/T) \tag{6}$$

Equation (2) for the volume emission rate can be written in the alternative form

$$\xi_\nu = 4\pi[O]k_\nu J_{\nu 0} \tag{7}$$

where the source function $J_{\nu 0}$ is $2c\nu_0^2\gamma/(1-\gamma)$. Note that $J_{\nu 0}$ is equal to Planck's function for the photon emission rate, at wavenumber ν_0, of a blackbody at temperature T.

The atmosphere is represented as a series of concentric shells, of vertical thickness 1 km, within which [O], T and p are constant. The integrals in equation (1) can be evaluated exactly for the contribution of each limb path segment Δz_i corresponding to a given shell (Fig. 1). The resulting expression for the limb spectral radiance is

$$N_\nu(H_T) = \sum_{i=1}^{N} \exp\left(-\sum_{j=i+1}^{N} \Delta\tau_{\nu j}\right)\left[1-\exp(-\Delta\tau_{\nu i})\right] J_{\nu 0 i} \tag{8}$$

where $\Delta\tau_{\nu i} = [O]_i\, k_{\nu i}\, \Delta z_i$ is the optical thickness of path segment Δz_i. A derivation of equation (8) from basic principles can be found in Bullitt, *et al.* (1985). They give

in addition an expression for the absorption coefficient that is applicable under general (LTE or non-LTE) conditions.

Collisional broadening has a very small effect on the integrated OI line radiances, which in the present application correspond to limb tangent heights $H_T \geq 90$ km. Even so, we used the Voigt rather than Doppler lineshape for $f(\nu)$. However, in calculating the collisional (Lorentz) width we used a fixed pressure profile, specifically, the one in the U.S. Standard Atmosphere (1976). With this procedure, the 147 μm and 63 μm limb radiance profiles computed from the above equations depend solely on the vertical profiles [O] vs. H and T(H). Retrieval of the [O] and T profiles involves a systematic fitting of computed 147 μm and 63 μm limb radiances to the corresponding measured limb radiances.

It should be noted that large errors in the retrieved [O] and T profiles would result if one were to assume an optically thin limb path, which would correspond to evaluating equation (8) in the limit as the $\Delta\tau$s approach zero. For example, the spectral transmittance at the center of the 63 μm line, between the tangent point and the observer at $z = Z$, is typically 0.007 for tangent height $H_T = 120$ km, and 0.95 for tangent height $H_T = 240$ km. The corresponding transmittances at the center of the 147 μm line are ~ 0.31 and ~ 0.98, respectively. If the objective or the radiative transfer calculation was merely to estimate $N_v(H_T)$ or $N(H_T)$, then the error resulting from the optically thin assumption would probably be judged acceptable above $H_T = 240$ km and

unacceptable below this tangent height. However, even the small error in $N(H_T)$ for $H_T > 240$ km would cause a very large error in the retrieved [O] and T profiles, as we shall demonstrate.

3. RETRIEVAL METHODOLOGY

The retrieval method to be described depends, physically, on differences in the local volume emission rate for the two OI lines. It has the capability to transform a pair of nonresolved limb radiance profiles $N(H_T)$ for the two lines into a pair of vertical profiles for the nonresolved volume emission rate,

$$\xi_n(H) = A_n \cdot [O] g_{un} \exp(-c_2 E_{un}/T)/Q(T); \quad n = 1,2 \qquad (9)$$

which is the rate given by equation (2) after integrating over the spectral line. In equation (9), n = 1 corresponds to the 147 μm line and n = 2 indicates the 63 μm line; [O] and T correspond to the same altitude as ξ_n. One can obtain T(H) from the ratio ξ_1/ξ_2:

$$R = \xi_1/\xi_2 = 0.0653 \exp[-97.84/T(H)] \qquad (10)$$

where we have used the values in Table 1 for the A_n, g_{un} and E_{un}. By using the inferred T(H) and ξ_1 or ξ_2, one can then determine [O]. Our retrieval method does not solve explicitly for $\xi_1(H)$ and $\xi_2(H)$, but obtains T and [O] more directly, as

described below. The method depends nonetheless on the sensitivity of the ratio R to temperature for the recovery of T(H), and on the sensitivity of ξ_1 and ξ_2 to [O] for the recovery of [O] vs. H. The value 97.84K appearing in equation (10) is the temperature-equivalent difference in upper state energies, equal to $c_2(E_{u1}-E_{u2})$.

From equation (10) we find that the error in temperature due to a relative error dR/R, if T were determined from this equation, is

$$dT = (T^2/97.84)\, dR/R \qquad (11)$$

The error dR would originate from noise in the limb radiance data and/or inevitable small errors in the solutions for ξ_1 and ξ_2. From equation (11), the value dR/R = 0.01 results in an error dT = 4K when T = 200K; the relative temperature error is only 4/200 = 0.02. If dR/R = 0.01 and T = 1200K, a temperature that can occur near 300 km altitude, the error dT is 147K; the relative error is 0.12. One can show similarly that the relative error d[O]/[O] is roughly three times dR/R or $d\xi/\xi$. Thus, it can be anticipated that temperatures can be recovered more accurately in the lower thermosphere than at, say 300 km, where the translational temperature will be large compared to the difference ($\sim$ 98K) between upper state energies; and that the O-atom density can be recovered to higher relative accuracy than the temperature over most of the thermosphere. Also, it is clear that the optically thin

assumption, while it would cause errors in R less than a few percent above 240 km, would lead to rather large errors in the recovered temperature above this altitude.

The retrieval algorithm used over most of the 90-300 km altitude range is based on the onion-peeling method, which is applied one layer at a time beginning at the top of the atmosphere. The solution values [O] and T for the layer at altitude $H = H_T$ are defined as those for which the function

$$F([O],T) = \sum_{n=1}^{2} \{[N_n(H_T) - \tilde{N}_n(H_T)]/\tilde{N}_n(H_T)\}^2 \qquad (12)$$

is a minimum. Again, subscript n distinguishes between the 147 μm and 63 μm lines; $N_n(H_T)$ denotes a computed limb radiance (integral of the spectral radiance), while $\tilde{N}_n(H_T)$ is the corresponding measured radiance. Thus, F([O],T) is a sum-square normalized difference between the predicted and measured limb radiances for the OI lines. Of course, $N_n(H_T)$ includes the net effects at the observation point $z = Z$ of all layers above altitude $H = H_T$, for which solutions [O],T have already been obtained. The procedure used to start the onion-peeling process and to estimate [O] and T for layers above the starting altitude (330 km) will be described subsequently.

The pair of least-squares normal equations obtained by formally minimizing F([O],T) are

$$\sum_{n=1}^{2} \partial N_n(H_T) / \partial \alpha_k [N_n(H_T) - \tilde{N}_n(H_T)] / \tilde{N}_n^2(H_T) = 0; \qquad (13)$$

$$k = 1, 2; \quad \alpha_1 = [O], \quad \alpha_2 = T$$

A solution [O],T of equations (13) is found using Newton's method. There is no solution when the determinant of the Jacobian matrix $\partial N/\partial \alpha$ is zero.

The term "layer," as used in the above description of the onion-peeling procedure, refers to specific index shells, one km in vertical thickness, whose altitudes differ by $\Delta H > 1$ km. For example, the tangent height H_T in equation (13), which is also the altitude of an index shell, will take on the value 150 km if H_T was 160 km in the previous cycle, since ΔH is defined to be 10 km for $H_T \geq 130$ km. A constraint on the solutions of equation (13) is that T and log[O] vary linearly with altitude between the two index layers, and connect with the [O],T solutions for the higher index layer. Thus, the onion-peeling cycle in which H_T is 150 km actually yields [O],T solution values for the ten shells at H = 159, 158, ..., 150 km. The guess values required by Newton's method are based on the presumption that the slope of T(H) and log[O] vs. H will not change from one cycle to the next. The retrieval algorithm uses ΔH = 4 km between 130 and 110 km altitude, and ΔH = 2 km below 110 km. These values are adequate to reproduce the structure of typical [O] and T vertical profiles. Note that the derivatives $\partial N_n(H_T)/\partial \alpha_k$ will

generally become smaller as ΔH is reduced, which will increase the potential for instability in the retrieval solutions due to noise (and/or propagation of noise and error).

The recovered temperature profile is smoothed above 130 km altitude by convolving it with a rectangular window function. Smoothing is performed, in each onion-peeling cycle, over the 20-km altitude range addressed in the two most recent cycles. Thus, each portion of the final T(H) solution above 130 km has been convolved twice with the boxcar, and exhibits no slope discontinuities.

The Jacobian referred to above was evaluated as a function of tangent height for two model [O],T profiles. These are the same models used to generate synthetic limb radiance data for testing the retrieval algorithm. The finite-difference Jacobian elements were based on perturbed [O],T profiles that differed from the model profiles only between H_T and H_T + 10 km, and that represented, over this 10-km region, linear T vs. H and linear log [O] vs. H. In other words, the numerical Jacobian values typified those which would occur in applying the onion-peeling algorithm to the synthetic limb radiance data. The Jacobian was found to be singular very near H_T = 200 km, but at no other H_T, for both models.

It is well known that the onion-peeling method tends to propagate noise. Hence, the T and [O] profiles recovered from noisey data can differ substantially from the true profiles near 200 km altitude, and consequently the Jacobian

singularity can occur at an altitude somewhat higher or lower than 200 km. This uncertainty in the location of the singularity tended to defeat the simple strategy of locating the index layers well away from the 200-km level, e.g., one at 220 km with the next lower one at 180 km. That is, successful solutions were a chance occurrence. However, it is notable that the onion-peeling procedure, whenever it did not fail because of the singularity, produced solutions down to $\sim$ 90 km altitude. In fact, the errors in the retrieved T and [O] profiles near $\sim$ 100 km altitude were generally much smaller than those above $\sim$ 180 km. It is apparent that the effects of noise propagation in the onion-peeling method are offset by (a) an increased sensitivity of the OI line radiances (ratio R) to temperature at the lower altitudes, where the atmosphere is cooler, and (b) higher signal-to-noise (a brighter limb) at the lower tangent heights.

As an alternative to the onion-peeling method, we considered the approach in which predicted OI radiances are fit to the measured radiances simultaneously for several tangent heights. By fitting at M tangent heights, it is possible to recover [O] and T simultaneously for $N \leq M$ altitudes. This method of retrieval is described by Carlotti (1988), who calls it the global-fit approach, and by Chang and Weinreb (1985), who refer to it as the Levenberg-Marquardt method after the algorithm they used to effect the nonlinear least-squares fit. We found that the global-fit method required considerable time on the CDC Cyber 860 computer when

it was used to recover [O] and T for just a few levels below the starting altitude; e.g., 600 sec was required when M = N = 3. Indeed, Carlotti (1988) describes a retrieval of stratospheric ozone concentrations by the global-fit approach that required substantial execution time on a Cray computer.

The algorithm finally adopted in the present study performs onion-peeling above 280 km altitude and below 180 km. The global-fit method is employed for the retrieval of [O] and T between these two altitudes. Specifically, we use a modified Levenberg-Marquardt algorithm (subroutine UNLSF in the International Math and Statistics Library) to fit simultaneously the measured limb radiances at H_T = 230 and 180 km and to obtain [O] and T at these two altitudes (i.e., M = N = 2), with the constraint that log[O] vs. H and T(H) are linear between 280 and 230 km and between 230 and 180 km. The function that is minimized is $F_1 + F_2$, where F_1 and F_2 are defined as F (Eq. 12) evaluated for H_T = 230 km and for H_T = 180 km, respectively. This procedure proved effective in avoiding the singularity at 200 km altitude for a wide range of noise levels in the synthetic data.

The starting procedure exploits the fact that above 250 km the translational temperature is nearly constant, while the O-atom density tends to fall off exponentially with altitude. Assuming these properties, and also that the limb above H_T = 250 km is optically thin, one can show that $N(H_T)$ is approximately exponential with the same scale height as [O] vs. H; see Sharma *et al.* (1988). In the starting procedure,

a single radiance scale height H_S is estimated from the two limb radiance profiles above H_T = 250 km, and is used to extrapolate the profiles from H_T = 300 (the largest value for which synthetic data was generated) to H_T = 330 km. The least-squares normal equations (13) are then solved for [O] and T at H = 330 km, using the two limb radiances for this tangent height. The constraint on the solution in this initial application of the normal equations is that T is constant and that d log[O]/dH equals the constant $-1/H_S$ above 330 km altitude. Thus, the solution defines T(H) and [O] vs. H for H $\geq$ 330 km. Note that the optically thin assumption, while it is used in this starting procedure to equate the scale heights of [O] and the limb radiance data $\tilde{N}(H_T)$, is not invoked in computing the predicted limb radiances $N(H_T)$ in equation (13).

Generally, there is some error in the T and [O] values obtained at H = 330 km due to the assumptions that T is constant and [O] is exponential above 250 km. The subsequent onion-peeling cycles tend to produce compensating errors that alternate in sign; i.e., the retrieved profiles exhibit oscillations. The oscillations usually decrease with each cycle and are very small when the altitude H = 280 km is reached. This is the reason for starting the retrieval at 330 km and for choosing 280 km as the highest level addressed by the global fitting procedure. After the T and [O] profiles are recovered, values above H = 290 km are discarded.

In summary, the retrieval is started at 330 km and is based on the described onion-peeling procedure, with a spacing of 10 km between index shells, down to 280 km. The global-fit technique, with index levels at 230 km and 180 km, is used to recover T and [O] between 280 and 180 km. The onion-peeling method is used below 180 km, with ΔH = 10 km above 130 km; ΔH is 4 km between 130 and 110 km and is 2 km below 110 km. Each 10-km section of the temperature profile above 130 km is smoothed twice regardless of which method is used to retrieve the section.

4. INVERSIONS OF SYNTHETIC DATA

Two models for the vertical profiles of O-atom density and translational temperature over the altitude range 90 to 300 km are shown in Fig. 2. These models, designated ATOI2 and ATOI4, were used to compute limb radiance profiles for the 147 μm and 63 μm OI lines, which are shown in Fig. 3. The limb radiance profiles, after addition of Gaussian noise, constitute the raw synthetic data to which a smoothing procedure and then the retrieval algorithm was applied.

The sensor system that would measure the limb radiance profiles (see Section 5) is envisioned to have a larger instantaneous field-of-view (IFOV) above 160 km than below this tangent height in order to provide a system noise-equivalent radiance (NER) five times smaller above H_T = 160 km. In other words, spatial resolution is traded for sensitivity at the higher tangent heights, where $N(H_T)$ is less

structured and is falling off rapidly. It is assumed that the instrument samples the OI limb radiances at intervals of 2 km in tangent height. Thus, we generated synthetic profiles at 2-km intervals, added noise samples corresponding to a given NER value (one-fifth this value above H_T = 160 km), and finally smoothed the profiles above H_T = 160 by convolving them with the 11-point cubic polynomial smoothing function given by Savitzky and Golay (1964). The 11 points of the smoothing function correspond to a total width of 20 km. The convolution was performed five times in succession, starting each time at a different tangent height, to effect smoothing above 160, 200, 220, 240 and 250 km, respectively. Smearing of the limb radiance profile by the finite instrument IFOV was not accounted for *per se*. However, above 160 km the smoothing procedure produces considerably more smearing than would result from the system IFOV. Note that the retrieval procedure uses only the limb radiances which correspond to the index levels defined earlier.

Retrievals were performed for the two synthetic data sets (corresponding to the models ATOI2 and ATOI4) for a wide range of NER values. The NER's used for the 63 μm limb radiances were always 0.6 times those used for the 147 μm limb radiances, corresponding to the relative detector/preamp-limited noise levels for the two sensor channels (see Section 5). Three retrievals were performed for each combination of atmospheric model and NER level; these correspond to three independent sets of Gaussian random

numbers for the noise samples. We will present results only for the highest NER levels that resulted in stable solutions, since it is these levels that define the required sensor performance.

Figure 4 shows the actual and retrieved [O],T profiles for atmospheric model ATOI2 when the system NER, for $H_T \leq 160$ km, is 10^{-12}W cm^{-2}sr^{-1} in the 147 μm channel and 6×10^{-13}W cm^{-2}sr^{-1} in the 63 μm channel. This is the highest noise level for which stable solutions could be obtained. In fact, in one of the six cases (6 = 2 models x 3 noise sets) corresponding to this noise level, the solution diverged at 160 km altitude; the other five solutions were stable down to 104 km (the altitude of the peak of the [O]-profile) or lower. Figure 5 shows the actual and retrieved [O],T profiles for model ATOI4 for the same NERs.

Figures 6 and 7 show typical results for models ATOI2 and ATOI4, respectively, when the NER's are half the above values, i.e., 5×10^{-13} and 3×10^{-13}W cm^{-2}sr^{-1}, respectively, for the 147 μm and 63 μm channels. In all six cases corresponding to this noise level, the solutions were stable down to 90 km altitude.

The four solutions display similar characteristics: The errors in retrieved temperature tend to be largest at the higher altitudes, specifically, where the actual temperature is greater than 600K. Even though these errors and noise are propagated by the onion-peeling procedure, the temperature solutions are remarkably stable at the lower altitudes. In

contrast, the errors in the retrieved O-atom density profile are significant only below the peak of the [O] profile . These errors are the result of noise and noise/error propagation in combination with the very high opacity of the 63 μm line below 120 km tangent height.

It may be noted that high signal-to-noise levels are required for successful retrievals. For example, the NER value of 5 x 10^{-13}W $cm^{-2}sr^{-1}$ for the 147 μm channel, which resulted in the [O],T solutions shown in Fig. 7, corresponds to S/N $\simeq$ 400 at tangent height 160 km, based on the signal levels given in Fig. 3. The NER value of 3 x 10^{-13}W $cm^{-2}sr^{-1}$ at 63 μm corresponds to S/N $\simeq$ 2 x 10^4 at H_T = 160 km. The latter S/N value is probably very much higher than needed for successful retrievals; it results from the fact that the signal (limb radiance) is much higher at 63 μm than 147 μm, while the detector-limited noise levels that can be achieved at the two wavelengths using Ga:Ge detectors are comparable.

5. CONCLUSIONS

Application of the described retrieval method to synthetic OI limb radiance data has established that vertical profiles of the atomic oxygen density and translational temperature can be successfully recovered over the altitude range 90 km to 300 km if the noise-equivalent radiance for the 147 μm channel is no greater than 5 x 10^{-13}W $cm^{-2}sr^{-1}$ for tangent heights $H_T \leq$ 160 km, and no greater than 10^{-13}W cm^{-2} sr^{-1} above 160 km. It is assumed that the 63 μm channel can

achieve NERs equal to 0.6 times these values, based on the fact that commercially available Ge:Ga photoconductive detectors can provide a noise-equivalent power (NEP) of $3 \times 10^{-17} W/Hz^{1/2}$ at 63 μm wavelength while a stressed detector of the same type can provide NEP = $5 \times 10^{-17} W/H^{1/2}$ at 147 μm. An additional requirement is that the sensor resolve the limb radiance profile to at least 2.5 km tangent height for $H_T \leq 160$ km. A tangent height footprint five times larger would suffice above 160 km tangent height.

Design goal data requirements, i.e., noise-equivalent radiances and instantaneous fields-of-view, are given in Table 2. The listed NERs are approximately three times lower than the maximum allowable values stated above. The listed IFOVs correspond to the requisite minimum tangent height resolutions if the sensor altitude is 300 km. The lower NERs for $H_T > 160$ km could be achieved, for example, by coadding the outputs of detectors in a five-by-five mosaic.

Figure 8 is a block diagram showing the principal components of a two-channel, non-scanning, cryogenic Fabry-Perot sensor to measure the OI limb radiance profiles. Design specifications for this sensor concept are listed in Table 3. The values given will provide, according to our calculations, the design goal NER's in Table 2. Note that the collecting telescope is 20 cm diameter and that the entire system operates at a temperature of 10K; the detectors must operate at 4K or lower. Coaddition of the 25 detector outputs is assumed for tangent heights greater than 160 km. Also, the

noise bandwidth of 1 Hz applies to a single pair (63 μm and 147 μm) of limb radiance samples. This implies roughly 100 seconds for measurement of the two limb radiance profiles, which is not an unreasonable value. Of course, tradeoffs are available among the parameters of Table 3, which represents a baseline model for engineering design of the sensor. It is also possible that detector NEP's lower than those in Table 3 will be available in the future.

The baseline model represents a system of reasonable size, with components that are well within current state-of-the-art technology. It is concluded that the experiment proposed by Sharma *et al* (1987), using the nonresolved measurement approach, and using the retrieval methodology described herein, is technically feasible.

Acknowledgments -- We gratefully acknowledge the interest and support of Randall Murphy at the Air Force Geophysics Laboratory and of the AFGL Commander, Col. J. R. Johnson. Valuable insights and motivation were provided by A. T. Stair, Jr. when he was Chief Scientist at AFGL. Howard Smith, when he was at the Naval Research Laboratory, helped us in analyzing Fabry-Perot system capabilities. This project was funded by the AFGL FY87 In-House Laboratory Research (ILIR) Program and was sponsored by the Air Force Systems Command through Contract No. F19628-87-C-0053. The United States Government is authorized to reproduce and distribute reprints for governmental purposes notwithstanding any copyright notation hereon.

Table 1. Parameters for the OI Transitions*

Transition	λ_0 (μm)	ν_0 (cm)	A (s^{-1})	E_u (cm^{-1})	g_u
$^3P_0 \rightarrow {}^3P_1$	147	68	1.705×10^{-5}	226.5	1
$^3P_1 \rightarrow {}^3P_2$	63	158.5	8.702×10^{-5}	158.5	3

*after Fischer and Saha 983).

Table 2. Design Goal NERs, IFOVs

Channel (μm)	Tangent height ≤ 160 km		Tangent height > 160 km	
	NER ($W\ cm^{-2}\ sr^{-1}$)	IFOV (mr x mr)	NER ($W\ cm^{-2}\ sr^{-1}$)	IFOV (mr x mr)
63	1.1×10^{-13}	1.5 x 1.5	2.2×10^{-14}	7.5 x 7.5
147	1.8×10^{-13}	1.5 x 1.5	3.6×10^{-14}	7.5 x 7.5

Table 3. Sensor Baseline Design Specifications

Instrument type	Two-channel Fabry-Perot interferometer (non-scanning)
Foreoptics	20 cm diameter, 5X magnification
Object-space IFOV	1.5 mr by 1.5 mr (each mosaic element)
Tangent height scan	90 km to 300 km, sampled at 2-km intervals
63 μm, 147 μm etalons	4 cm effective diameter, 4.7 cm actual diameter Resolving power $\simeq$ 1000 Maximum emissivity $\simeq$ 0.1
Blocking filters	1 μm width
System optical efficiency	0.4 minimum
Noise bandwidth	1 Hz (each limb radiance sample)
System temperature	10K (detectors at 4K)
Focal planes	5 x 5 element mosaic, 0.136 cm x 0.136 cm each element
63 μm detectors	Ga:Ge with NEP = $3 \times 10^{-17} W/Hz^{1/2}$ maximum
147 μm detectors	Stressed Ga:Ge with NEP = $5 \times 10^{-17} W/Hz^{1/2}$ maximum

REFERENCES

Bates, D. R. (1951) The temperature of the upper atmosphere. *Proc. Phys. Soc.* 64b, 805.

Bullitt, M.K., Bakshi, P. M., Picard, R. H. and Sharma R. D. (1985) Numerical and analytical study of high-resolution limb spectral radiance from nonequilibrium atmospheres. *J. Quant. Spectrosc. Radiat. Transfer.* 34, 33.

Carlotti, M. (1988) Global-fit approach to the analysis of limb-scanning atmospheric measurements. *Appl. Optics.* 27, 3250.

Chang, I-Lok and Weinreb, M. P. (1985) Retrieval calculations applied to solar occultation measurements, in *Advances in Remote Sensing Retrieval Methods*, A. Deepak, H. E. Fleming and M. T. Chahine (Eds.), p 149. A. Deepak Publishing, Hampton, VA.

Fischer, C. F. and Saha, H. P. (1983) Multiconfigurational Hartree-Fock results with Breit-Pauli corrections for forbidden transitions in the $2p^4$ configuration. *Phys. Rev. A.* 28, 3169.

Goldman, A. and Saunders, R. S. (1979) Analysis of atmospheric infrared spectra for altitude distribution of atmospheric trace constituents - I: method of analysis. *J. Quant. Spectrosc. Radiat. Transfer.* 21, 155.

Savitsky, A. and Golay, M. J. E. (1964) Smoothing and differentiation of data by simplified least squares procedures. *Anal. Chem.* 36, 1627. Corrections to some of the tables are given by Steinier, *et al.* (1972), *Anal. Chem.* 44, 1909.

Sharma, R. D., Stair, A. T. Jr., and Smith, H. A. (1987) A spaceborne passive infrared experiment for remote sensing of the atomic oxygen density and temperature, and total density in the upper atmosphere. *Adv. Space Res.* 7, 31.

U.S. Standard Atmosphere (1976) National Oceanic and Atmospheric Administration, National Aeronautics and Space Administration, United States Air Force, Washington, DC (October 1976).

Zachor, A. S. and Sharma, R. D. (1989) Retrieval of atomic oxygen and temperature in the thermosphere. 1: feasibility of an experiment based on the spectrally resolved 147 μm limb emission. *Planet. Space Sci.* __, .

FIGURE CAPTIONS

1.) Coordinates and parameters involved in calculating the limb spectral radiance (see text).

2.) Two models for the vertical profiles of atomic oxygen density and translational temperature. They represent a cool thermosphere (model ATOI2, represented by dashed curves) and a relatively warm thermosphere (model ATOI4, full lines).

3.) OI limb radiance profiles calculated for the two models shown in Fig. 2. The dashed lines correspond to model ATOI2, the full lines to model ATOI4.

4.) Actual (full lines) and retrieved (dashed lines) profiles of [O],T for atmospheric model ATOI2. The noise-equivalent radiances for the 147 μm and 63 μm channels are 10^{-12} W $cm^{-2}sr^{-1}$ and 6 x 10^{-13} W $cm^{-2}sr^{-1}$, respectively.

5.) Same as Fig. 4, except the atmospheric model is ATOI4.

6.) Same as Fig. 4, except the NERs for the 147 μm and 63 μm channels are 5 x 10^{-13} W $cm^{-2}sr^{-1}$ and 3 x 10^{-13} W $cm^{-2}sr^{-1}$, respectively.

7.) Same as Fig. 6, except the atmospheric model is ATOI4.

8.) Sensor block diagram for the nonresolved, two-color concept.

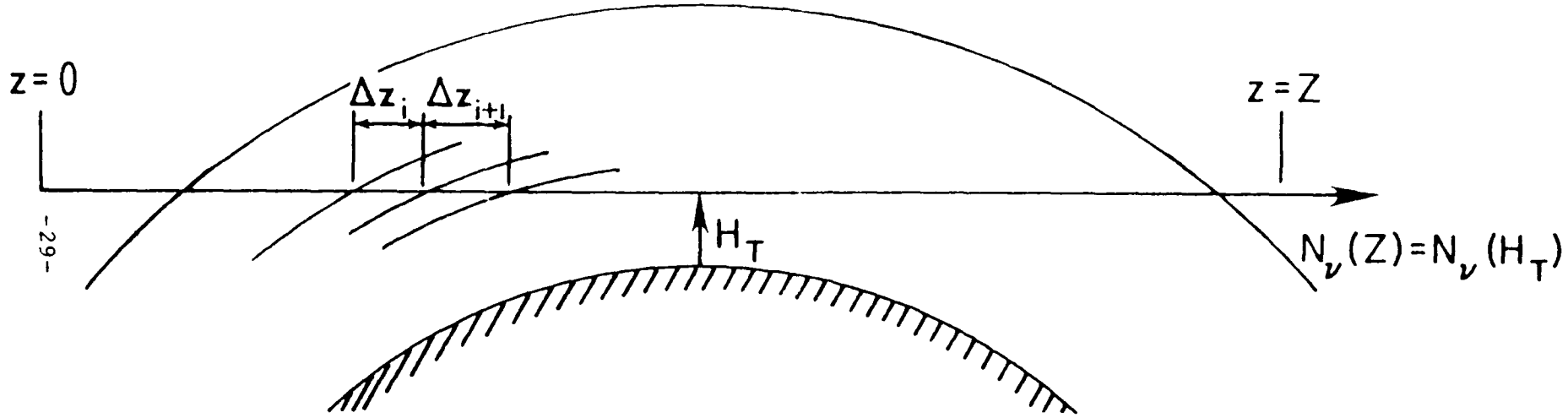

FIGURE 1

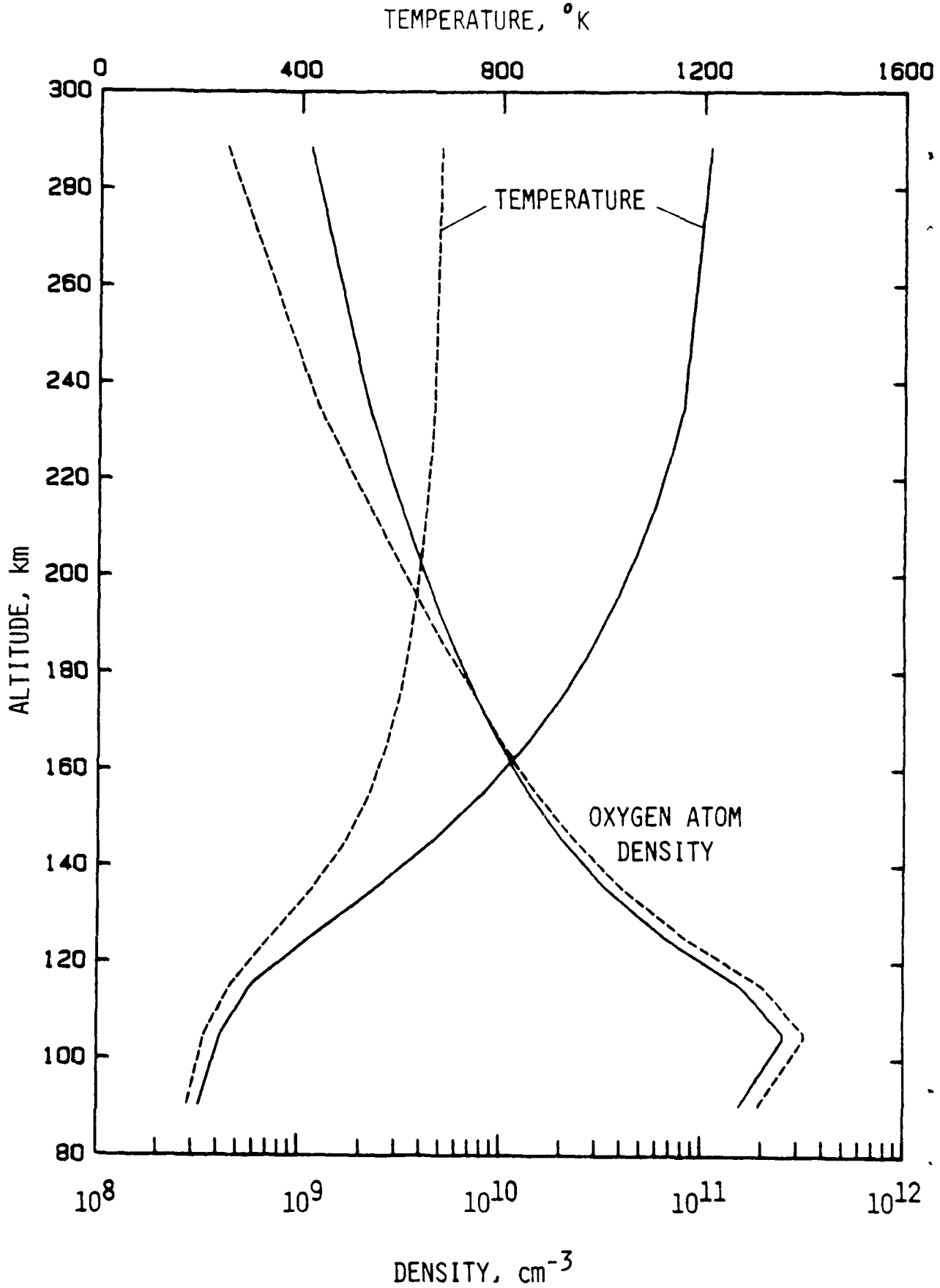
TEMPERATURE, °K
0
400
800
1200
1600
300
280
260
240
220
200
180
160
140
120
100
80
ALTITUDE, km
TEMPERATURE
OXYGEN ATOM
DENSITY
10^8
10^9
10^{10}
10^{11}
10^{12}
DENSITY, cm^{-3}

FIGURE 2

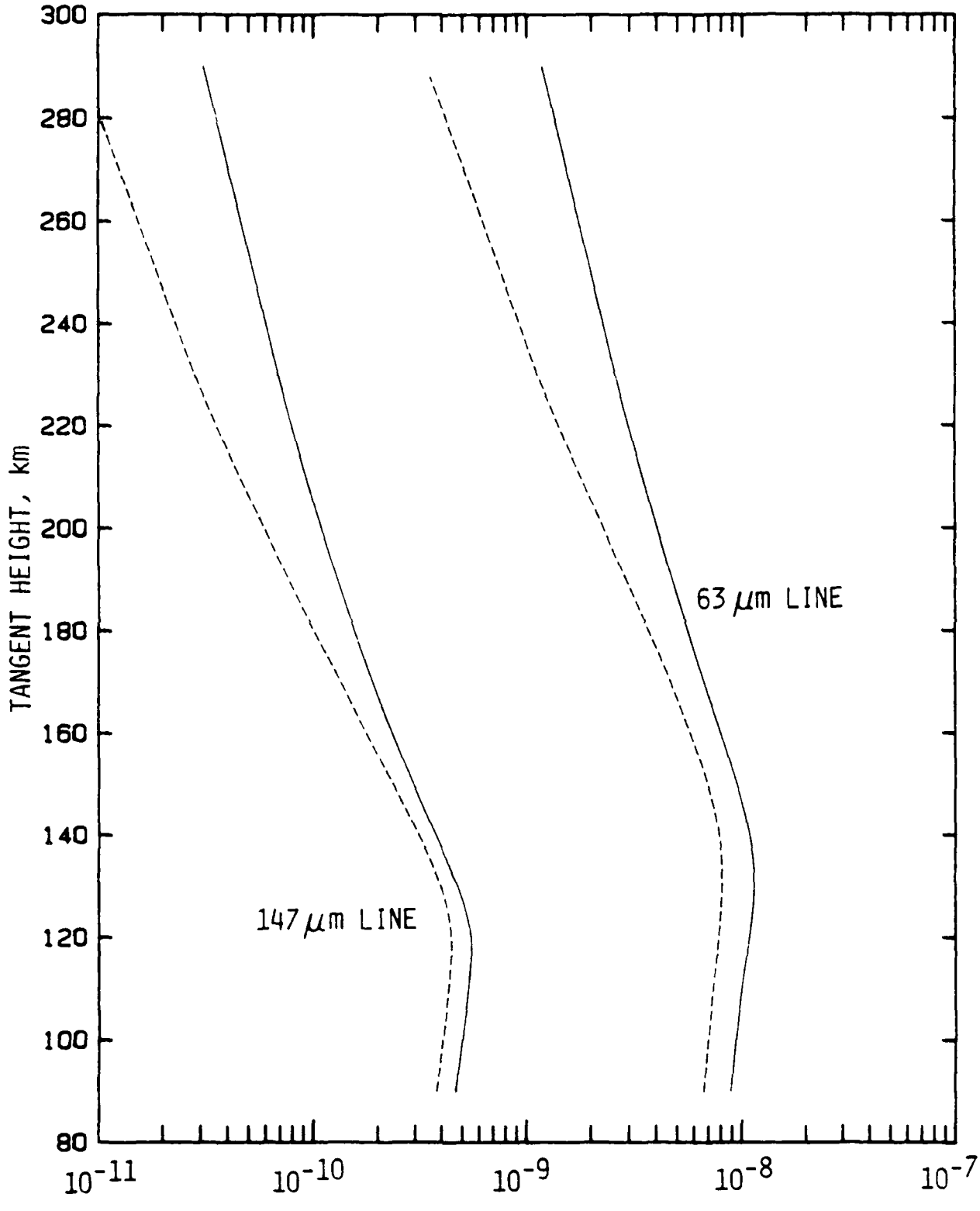
300
280
260
240
220
200
180
160
140
120
100
80
TANGENT HEIGHT, km
63 μm LINE
147 μm LINE
10^-11
10^-10
10^-9
10^-8
10^-7
RADIANCE, W cm^-2 sr^-1

FIGURE 3

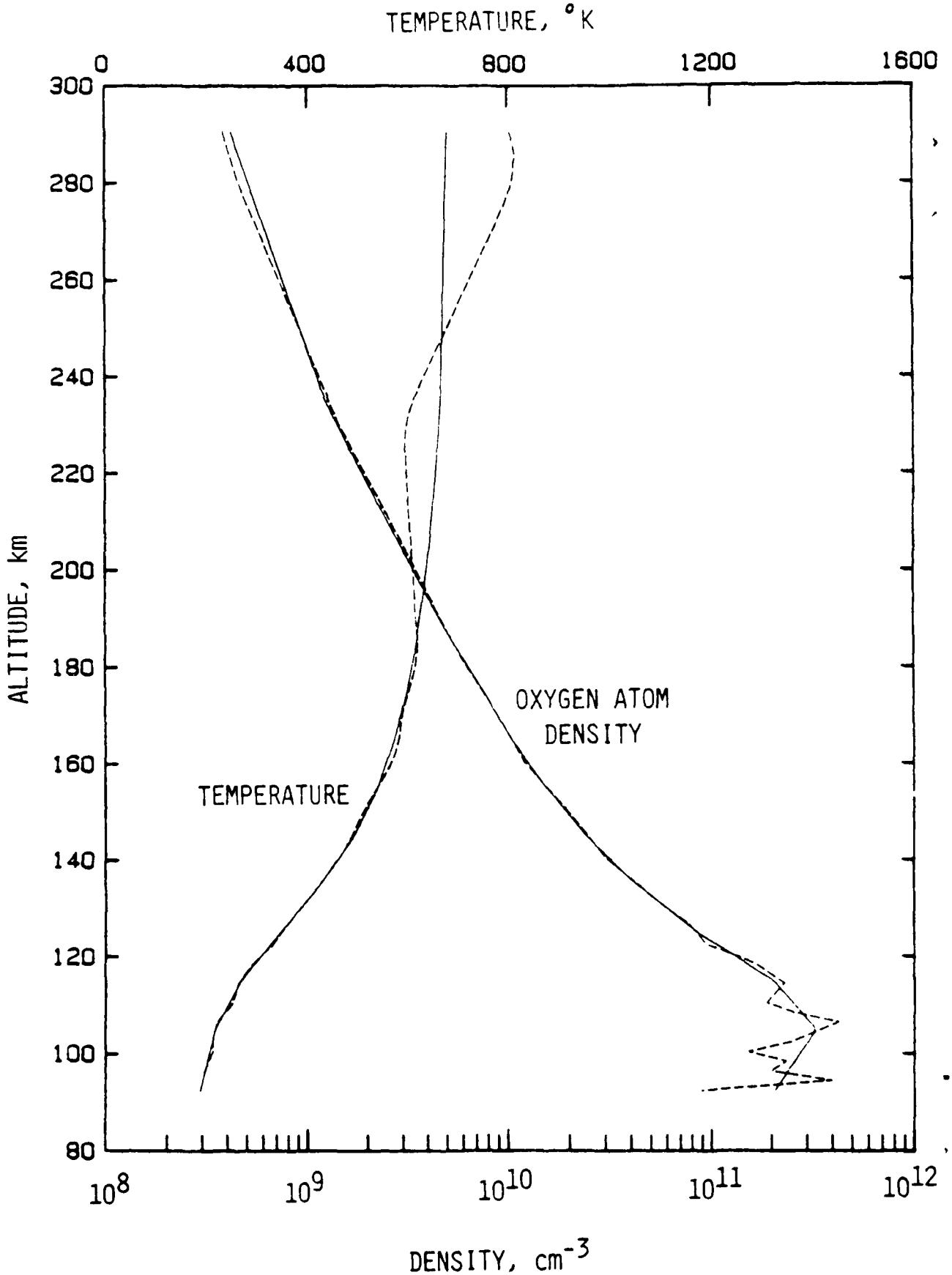
TEMPERATURE, °K
0
400
800
1200
1600
300
280
260
240
220
200
180
160
140
120
100
80
ALTITUDE, km
OXYGEN ATOM
DENSITY
TEMPERATURE
10^8
10^9
10^{10}
10^{11}
10^{12}
DENSITY, cm^{-3}

FIGURE 4

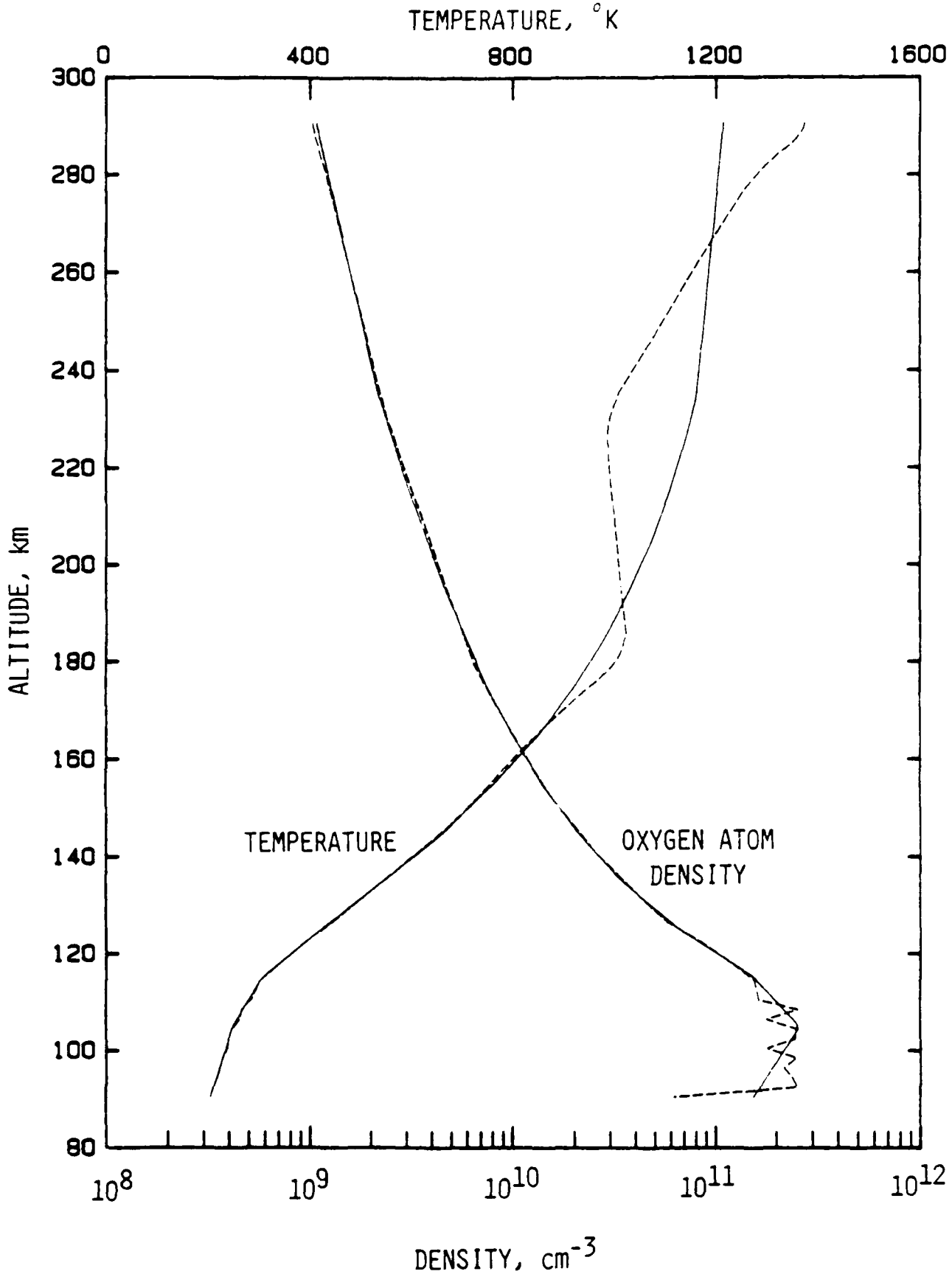
TEMPERATURE, °K
0
400
800
1200
1600
300
280
260
240
220
200
180
160
140
120
100
80
ALTITUDE, km
TEMPERATURE
OXYGEN ATOM
DENSITY
10^8
10^9
10^{10}
10^{11}
10^{12}
DENSITY, cm^{-3}

FIGURE 5

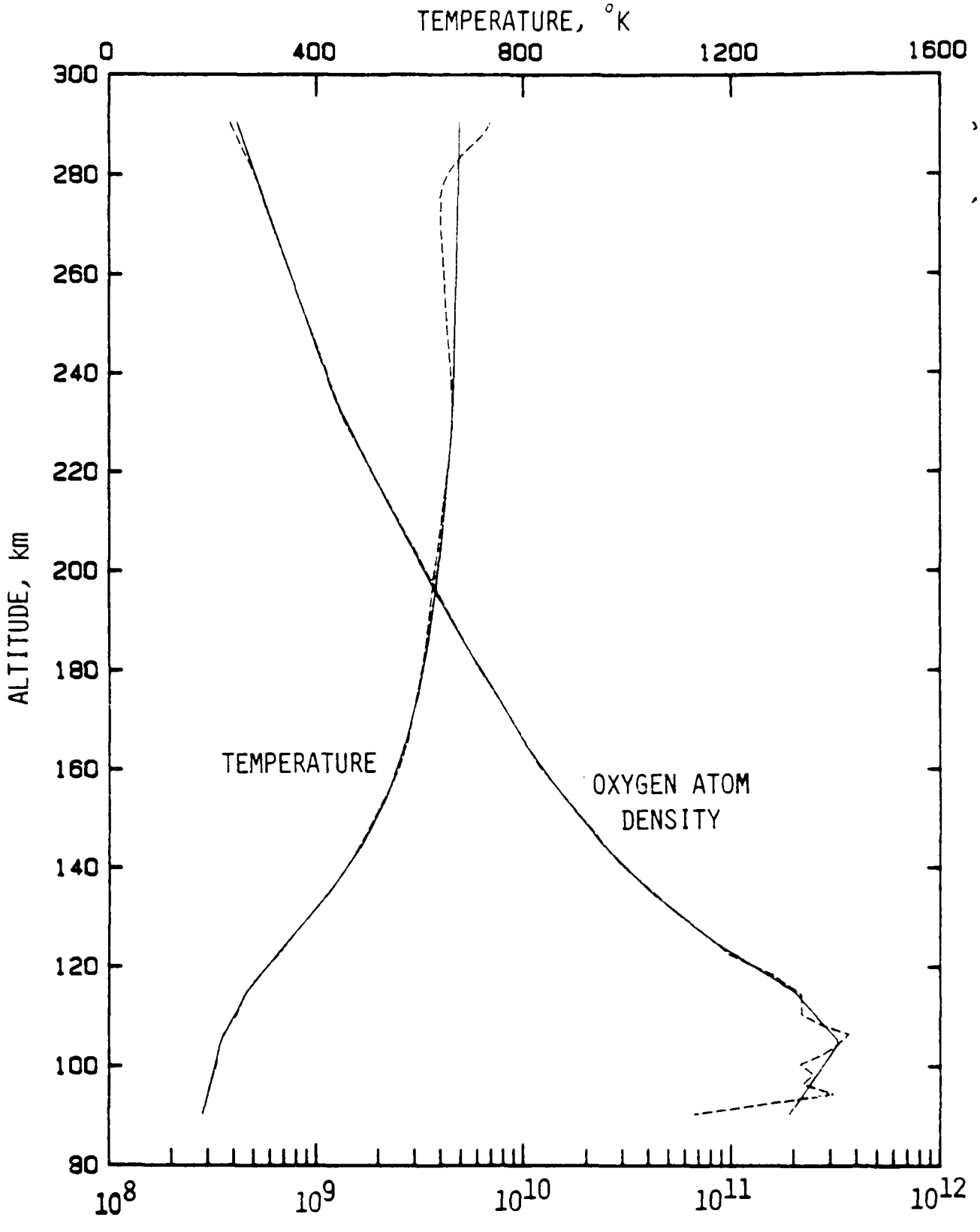
TEMPERATURE, °K
0
400
800
1200
1600
300
280
260
240
220
200
180
160
140
120
100
80
ALTITUDE, km
TEMPERATURE
OXYGEN ATOM
DENSITY
10^8
10^9
10^{10}
10^{11}
10^{12}
DENSITY, cm^{-3}

FIGURE 6

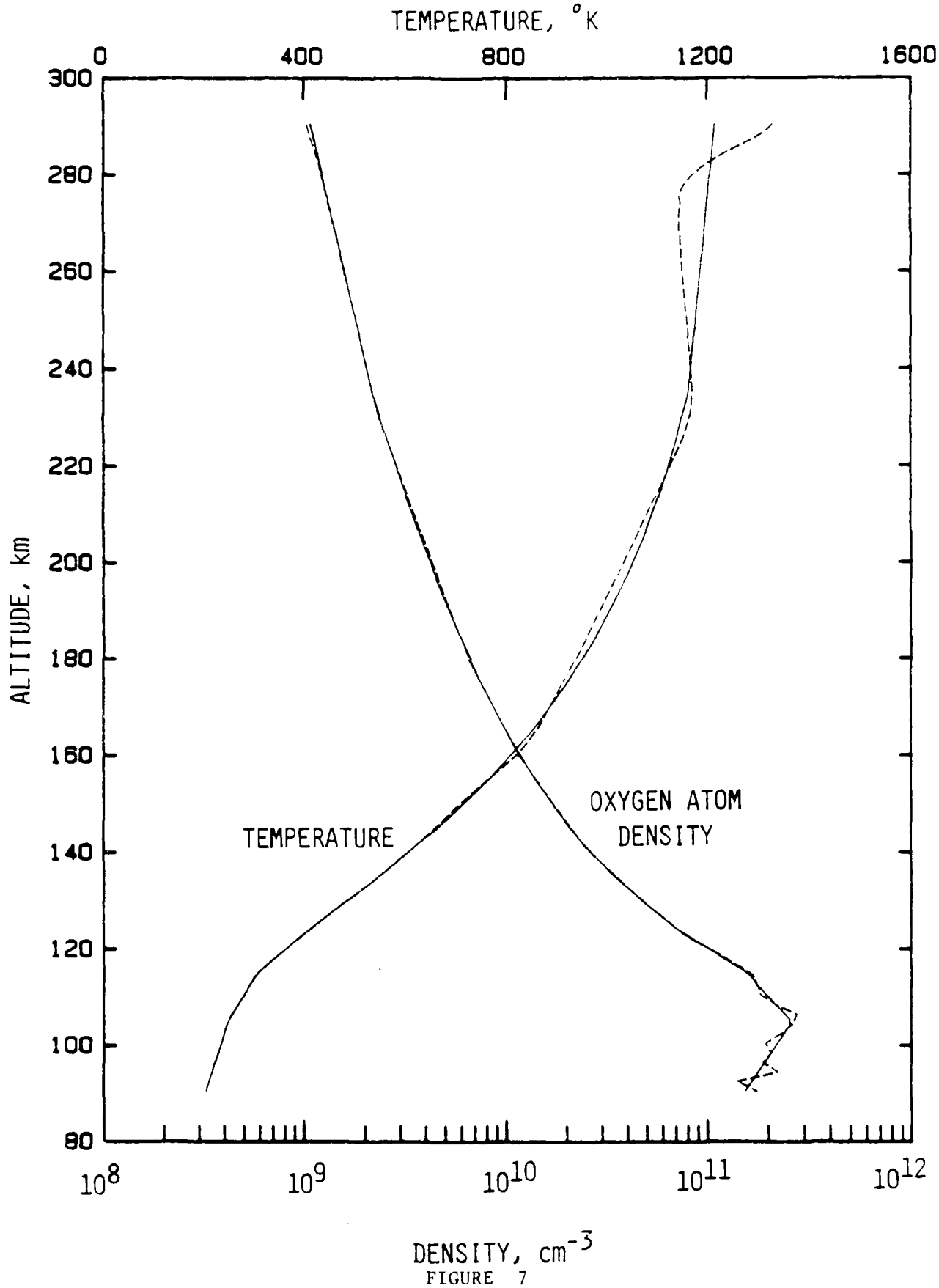
TEMPERATURE, °K
0
400
800
1200
1600
300
280
260
240
220
200
180
160
140
120
100
80
ALTITUDE, km
TEMPERATURE
OXYGEN ATOM
DENSITY
10^8
10^9
10^{10}
10^{11}
10^{12}
DENSITY, cm^{-3}

FIGURE 7

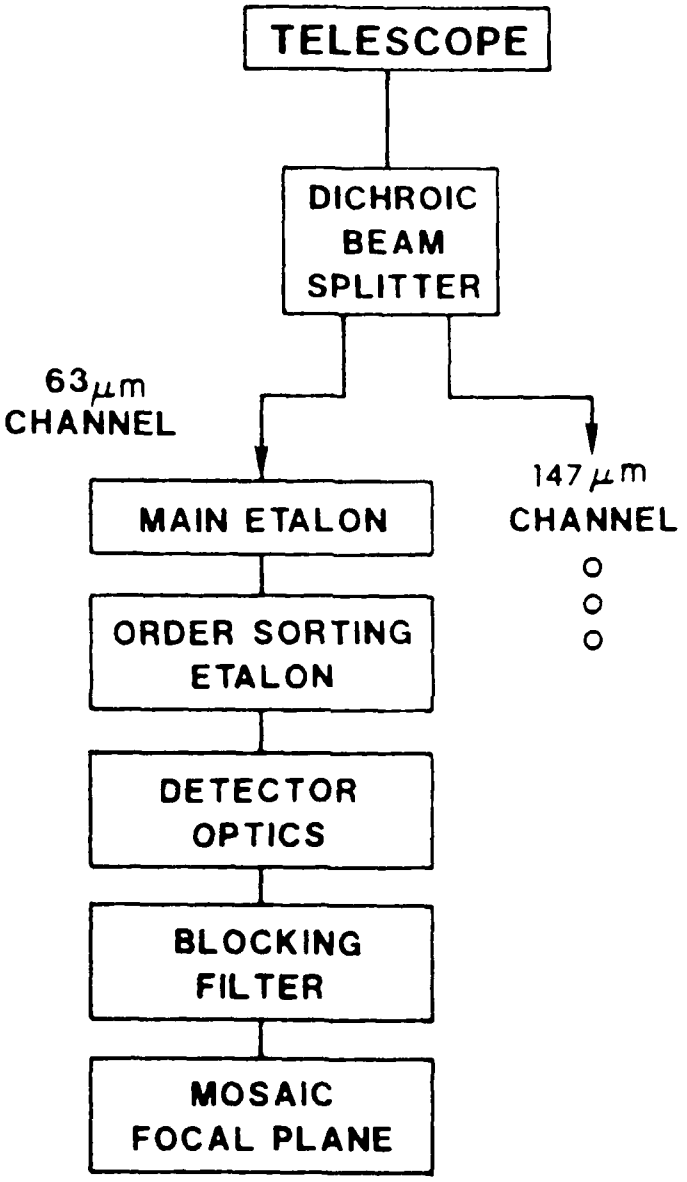
TELESCOPE
DICHROIC BEAM SPLITTER
63 μm CHANNEL
147 μm CHANNEL
MAIN ETALON
ORDER SORTING ETALON
DETECTOR OPTICS
BLOCKING FILTER
MOSAIC FOCAL PLANE

FIGURE 8